BIOCHEMISTRY
including biophysical chemistry & molecular biology

Article

pubs.acs.org/biochemistry

Platinated DNA Affects Zinc Finger Conformation. Interaction of a Platinated Single-Stranded Oligonucleotide and the C-Terminal Zinc Finger of Nucleocapsid Protein HIVNCp7

Susana Quintal,[†,‡] Aldino Viegas,[‡] Stefan Erhardt,[‡] Eurico J. Cabrita,[‡] and Nicholas P. Farrell*[,†]

[†]Department of Chemistry, Virginia Commonwealth University, P.O. Box 842006, Richmond, Virginia 23284, United States
[‡]REQUIMTE, CQFB, Departamento Química, FCT-UNL, 2829-516 Caparica, Portugal

Supporting Information

ABSTRACT: This paper describes for the first time the intimate molecular details of the association between a platinated oligonucleotide and a zinc finger peptide. Site-specific platination of the guanine in a single-stranded hexanucleotide gave {[Pt(dien)d(5′-TACGCC-3′)], Pt(dien)(6-mer)} (**II**) characterized by mass spectrometry and ^{1}H nuclear magnetic resonance (NMR) spectroscopy. The work extends the study of platinum−nucleobase complex−zinc finger interactions using small molecules such as [Pt(dien)(9-EtGua)]$^{2+}$ (**I**). The structure of the (34−52) C-terminal finger of HIV nucleocapsid protein HIVNCp7 (**ZF1**) was characterized by ^{1}H NMR spectroscopy and compared with that of the N-terminal single finger and the two-finger "intact" NCp7. Interaction of **II** with **ZF1** results in significant changes in comparison to the "free" uncomplexed hexanucleotide; the major changes occurring for Trp37 resonances that are broadened and moved upfield, and other major shifts are for Gln45 (Hε21, Hγ3, Qβ), Met46 (NH, Hγ2), Lys47 (NH, Qγ), and Glu50 (Hγ2, Hγ3). The Zn−Cys/His chemical shifts show only marginal deviations. The solution structures of **ZF1** and the 6-mer−**ZF1** and **II**−**ZF1** adducts were calculated from the nuclear Overhauser effect spectroscopy-derived distance constraints. The DNA position in the **II**−**ZF1** adduct is completely different than in the absence of platinum. Major differences are the appearance of new Met46−Cyt6 H5 and Trp37−Cyt5 H5 contacts but severe weakening of the Trp37−Gua4 contact, attributed to the steric effects caused by Gua4 platination, accompanied by a change in the position of the aromatic ring. The results demonstrate the feasibility of targeting specific ZF motifs with DNA-tethered coordination compounds, such as Pt compounds and Co macrocycles, with implications for drug targetting and indeed the intimate mechanisms of DNA repair of platinated DNA.

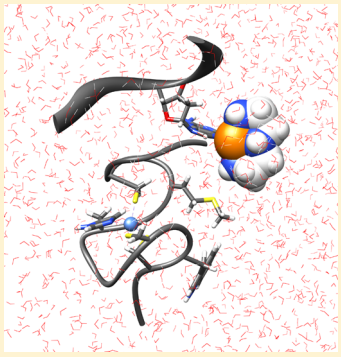

The zinc finger motif represents 1−3% of the human genome.[1] Zinc finger (ZF) proteins are important targets for antiviral and anticancer drug interventions.[2] As a general strategy, modification of the zinc-binding site through electrophilic attack (alkylation or oxidation) on the nucleophilic zinc−thiolate bond and/or zinc chelation results in a loss of tertiary structure and inhibition of function (DNA−RNA binding). Nucleocapsid protein NCp7 of human immunodeficiency virus type 1 (HIV-1) contains two highly conserved zinc finger domains that are necessary for viral replication with a high affinity for nucleic acids and participate directly in multiple aspects of genome recognition and encapsidation.[3] As such, it is an attractive target for anti-HIV therapy, capable of complementing the activity of drugs already clinically used in HAART (highly active antiretroviral therapy).[4] Various classes of organic-based molecules have been extensively studied on this basis.[5−7]

Coordination compounds in general act as electrophiles toward ZFs with implications for new anticancer and antiviral drug design.[2] Small molecules such as *cis*-[PtCl$_2$(NH$_3$)$_2$] (cisplatin), *trans*-[PtCl(9-EtGua)(pyr)$_2$]$^{+}$, and [PtCl(dien)]$^{+}$ bind to various discrete ZFs, disrupting protein conformation with eventual Zn loss.[8−11] Specifically, a novel small molecule approach to targeting the retroviral zinc finger−DNA interaction uses the electrophilic nature of platinum−nucleobase compounds.[9] The displacement of Zn in the C-terminal (34−52) finger of HIV NCp7 [**ZF1** (Figure 1)] by monofunctional platinum−nucleobase compounds such as *trans*-[PtCl(9-EtG)(pyr)$_2$]$^{+}$ and [*SP*-4-2][PtCl(9-EtG)(NH$_3$)(quin)]$^{+}$ is consistent with the incipient antiviral activity of these species.[9] The moderate antiviral selectivity and relatively noncytotoxic properties of these compounds are in contrast to the high cytotoxicity shown by the parent dichlorides *trans*-[PtCl$_2$(pyr)$_2$] and *trans*-[PtCl$_2$(NH$_3$)(quin)].

An inherent challenge in the use of small molecule electrophiles to inhibit protein function is selectivity. In this respect, the details of the zinc finger−nucleotide interaction can be examined for systematic approaches to drug design. Hydrophobic, electrostatic, and hydrogen bonding interactions all contribute to the stabilization of the nucleocapsid−nucleic acid complex. A key molecular recognition feature is based on

Received: December 12, 2011
Revised: February 2, 2012
Published: February 3, 2012

dx.doi.org/10.1021/bi201834g | *Biochemistry* 2012, 51, 1752−1761

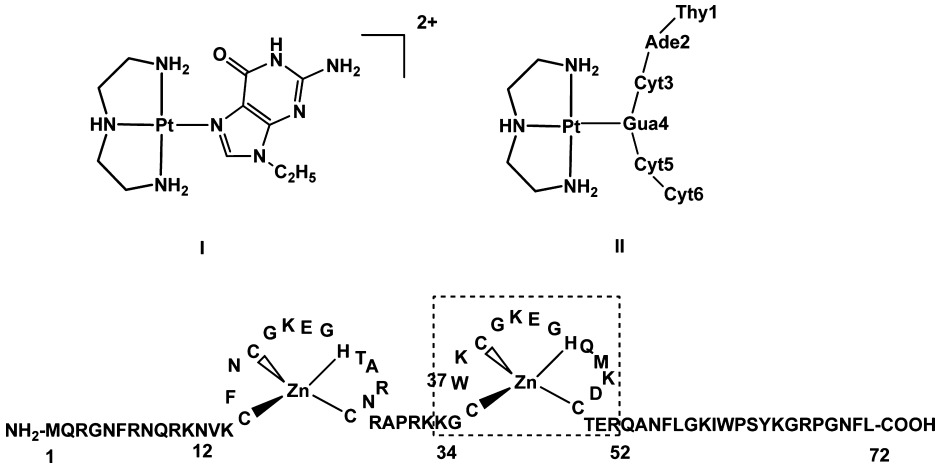

Figure 1. Structures of $[Pt(dien)(9\text{-EtG})]^{2+}$ (**I**), {[Pt(dien)d(5′-TACGCC-3′)], Pt(dien)(6-mer)} (**II**), and the entire HIV nucleocapsid protein. The site of DNA platination is denoted Gua4. The (34−52) C-terminal finger used in this study (**ZF1**) is shown in a dashed box.

Table 1. Structural Statistics for the 20 NMR Structures of ZF1 and 6-mer/ZF1 and II/ZF1 Mixtures

	ZF1	6-mer/ZF1	II/ZF1
no. of distance restraints			
total distance restraints from NOEs	290	394	418
short-range ($\|i-j\| \leq 1$)	196	217	254
medium-range ($1 < \|i-j\| < 5$)	49	60	68
long-range ($\|i-j\| \geq 5$)	45	117	96
zinc distance restraints	4	4	4
CYANA statistics (20 structures)			
target function	0.08	2.15	1.25
maximal distance violation (Å)	0.11	0.82	0.72
average backbone rmsd	0.62	0.24	0.37
average heavy atom rmsd	1.35	0.67	0.94
Ramachandran plot analysis (%)			
favorable	63.9	60.2	70.0
additional	33.2	38.3	28.2
generous	2.9	1.5	1.8
nonfavorable	0.0	0.0	0.0

the π-stacking between purine (guanine and adenine) nucleic acid bases and aromatic amino acid residues tryptophan and phenylalanine, as exemplified by interactions between Trp37 and guanine bases in interactions of NCp7 with small oligonucleotides such as d(5′-ACGCC-3′) and larger stem−loop SL3 ψ-RNA.[12−14] The interaction of $[Pt(dien)(9\text{-EtGua})]^{2+}$ (**I**) with **ZF1** is a model for "noncovalent" molecular recognition based on the "natural" biological motif of purine/pyrimidine−tryptophan interactions (see Figure 1).[8] Platination (metalation) of purine nucleobases, in analogy to alkylation, enhances stacking overlap with aromatic amino acids such as tryptophan, and this recognition feature may be modulated by the nature of the metal coordination sphere.[8,15,16] Fluorescence and mass spectrometric studies were consistent with $\pi-\pi$ stacking of the platinum−guanine moiety in **I** with the tryptophan of **ZF1**.[8] The association constants with **ZF1** from fluorescence studies using Eadie−Hofstee analysis for $[Pt(dien)(9\text{-EtGua})]^{2+}$ and the 5′-guanosine monophosphate analogue $[Pt(dien)(GMP)]^{+}$ of 7.5 and 12.4 × 10^3 M^{-1}, respectively, compare favorably with the value of 60.0 × 10^3 M^{-1} found for the single-stranded (ss) hexanucleotide d(TACGCC).[8] ^{1}H nuclear magnetic resonance (NMR) spectroscopic studies of the binding of hexanucleotide d(TACGCC) to **ZF1** were consistent with destacking of the cytosine from the nucleic acid single strand rather than a formal intercalation of the tryptophan ring between the adjacent C_3 and G_4 bases. The results are very similar to those for ZF protein NCp10 of Moloney leukemia virus and d(ACGCC).[17] It was therefore of interest to examine how platination of small oligonucleotide sequences can affect zinc finger interactions and interruption of the nucleic acid chaperone function of the protein. DNA-conjugated cobalt−Schiff base complexes have been designed to attack zinc-bound histidine in a zinc finger-selective manner.[18,19] This paper describes for the first time the intimate molecular details of the association between a platinated oligonucleotide {[Pt(dien)d(5′-TACGCC-3′)], Pt(dien)(6-mer)} (**II**) with **ZF1** (Figure 1).

EXPERIMENTAL PROCEDURES

Sample Preparation. The complex [PtCl(dien)]Cl (dien = diethylenetriamine) was prepared according to the literature procedure.[20] Oligonucleotide d(5′-TACGCC-3′) (6-mer) was purchased from The Midland Certified Co., Inc.. and peptide KGCWKCGKEGHQMKDCTER was from GenScript. **ZF1** was synthesized using the reported method and characterized by TOF ESI-MS (Figure S1 of the Supporting Information) and ^{1}H NMR in D_2O and a 90% Milli-Q H_2O/10% D_2O mixture.[8]

dx.doi.org/10.1021/bi201834g | *Biochemistry* 2012, 51, 1752−1761

II was synthesized by reacting the 6-mer with [PtCl(dien)]Cl in a 10 mM $NaClO_4$ aqueous solution at 37 °C. The reaction was followed by fast performance liquid chromatography (FPLC) on a strong anionic Mono Q 5/50 GL column (Pharmacia Biotech system) with a 0.05 to 0.8 M NaCl gradient in 10 mM Tris buffer (pH 7.4). After 24 h, the product was collected, extensively dialyzed against H_2O at 4 °C, lyophilized; and characterized by TOF ESI-MS and NMR spectroscopy (Figures S1 and S2 of the Supporting Information).

NMR Spectroscopy. The samples for NMR experiments were lyophilized twice from 99.96% D_2O and redissolved in 99.96% D_2O, and the pD was adjusted to 5.7 with NaOD. For H_2O NMR spectra, the D_2O solutions were lyophilized and redissolved in a 90% Milli-Q H_2O/10% D_2O mixture, and the pD was adjusted to 5.7 with NaOD or DNO_3. NMR spectra were recorded at 298 K on a Varian Unity 400 MHz or a Bruker Avance III 600 MHz (Bruker, Wissembourg, France) instrument equipped with a 5 mm inverse detection triple-resonance z-gradient probe. One-dimensional (1D) ^{1}H NMR spectra were recorded employing a 14423.077 Hz spectral width, with 32K data points. Water suppression was achieved by using excitation sculpting with gradients.[21]

To assign the nonexchangeable protons of free ZF1 and the 6-mer/**ZF1** and **II**/**ZF1** mixtures, spectra were acquired via standard two-dimensional (2D) gDQ-COSY, total correlation spectroscopy (TOCSY), and nuclear Overhauser effect spectroscopy (NOESY). The 2D gDQ-COSY spectra were acquired with eight scans and 4096 points in the direct dimension and 1024 increments. The 2D TOCSY spectra were acquired with eight scans and 4096 points in the direct dimension and 512 increments. The mixing time was set to 80 ms, and the time domain data were zero filled to yield a 2048 × 1024 data matrix. The 2D NOESY spectra were acquired with eight scans and 2048 points in the direct dimension and 512 increments. The mixing time was set to 60 ms, and the time domain data were zero filled to yield a 2048 × 1024 data matrix. For all spectra, the spectral width was 9615.385 Hz in both dimensions and the central frequency was set on the solvent signal (water). Long-range ^{15}N HSQC spectra provided connectivities between ^{1}H and ^{15}N atoms in the ring of the single His residue and were acquired with 2048 × 256 points and 512 scans. The spectral widths were 14423 Hz for ^{1}H and 12164 Hz for ^{15}N. The central frequency for the proton was set on the solvent signal (water) and for nitrogen was set on the center of the aliphatic amine region. All spectra were analyzed with Topspin2.0 (Bruker). Assignment and cross-peak area calculations were performed with Sparky by using the classical NOE-based methodology.[22,23]

Interaction of ZF1 with 6-mer and {Pt(dien)(6-mer)}. The interaction of free **ZF1** with 6-mer and **II** was studied by NMR chemical shift perturbations. For this study, natural abundance ^{1}H−^{15}N HSQC spectra of free **ZF1** and 6-mer/**ZF1** and **II**/**ZF1** mixtures were acquired with 2048 × 256 points and 256 scans. The spectral widths were 9615 Hz for ^{1}H and 2311 Hz for ^{15}N. The central frequency for the proton was set on the solvent signal (water) and for nitrogen was set on the center of the amide region.

To evaluate the behavior of individual amino acids upon addition of 6-mer and **II**, we have calculated the combined chemical shift differences using eq 1:[24]

$$\Delta\delta_{comb} = \sqrt{(\Delta\delta_H)^2 + (w_i\Delta\delta_N)^2} \quad (1)$$

where $\Delta\delta_H$ and $\Delta\delta_N$ are the chemical shifts of the proton and nitrogen, respectively, and w_i is a weighting factor that accounts for differences in sensitivity of different resonances in an amino acid (e.g., amide ^{1}H and ^{15}N). The weighting factors are given by

$$w_t = \frac{|\gamma_i|}{|\gamma_H|} \quad (2)$$

with γ_i and γ_H being the magnetogyric ratios of nucleus i and the proton, respectively. For the calculation of the cutoff value, we have used the corrected standard deviation to zero σ_0^{corr}.[24]

Structure Calculation. After the assignments had been completed, peaks from NOESY spectra were analyzed in a semiautomated iterative manner with CYANA2.1.[25] The NOE coordinates and intensities used as input for automated analysis were generated automatically with Sparky. This information was used by CYANA/CANDID to compute seven cycles of NOE cross-peak assignment and structure calculation, each with 100 starting structures. A Zn atom was added to the CYANA library as a replacement for H_γ of residue Cys36, and specific distance constraints were imposed for the Zn(II) coordination by residues Cys36, Cys39, Cys49, and His44 [Zn−S_γ (2.25−2.35 Å) and Zn−$N_{\varepsilon 2}$ (1.95−2.05 Å)].[26] The long-range ^{15}N HSQC spectrum provided connectivities between ^{1}H and ^{15}N atoms in the ring of the single His residue, and the observed $N_{\varepsilon 2}$−$H_{\varepsilon 1}$, $N_{\varepsilon 2}$−$H_{\delta 2}$, and $N_{\delta 1}$−$H_{\varepsilon 1}$ cross-peaks clearly established the presence of the $N_{\delta 1}$−H tautomer.[27] These results, along with the $^{15}N_{\varepsilon 2}$ and $^{15}N_{\delta 1}$ chemical shifts, indicated that the zinc ion is coordinated to $N_{\varepsilon 2}$. Input data and structure calculation statistics are summarized in Table 1.

The 20 conformers with the lowest final CYANA target function values were further subjected to restrained energy minimization in a water shell by using the AMBER 9.0 package,[28] using the ff99SB all atom force field.[29] The complex was immersed in an octahedral box using the TIP3P water model,[30] with a thickness of 10 Å. Counterions were also included to neutralize charge, and a total of four sodium ions were added. The simulation was performed by using periodic boundary conditions and the particle mesh Ewald approach to account for the electrostatic interactions.[31] The restrained energy minimization was performed in three stages. In the first stage, the solvent molecules were minimized by MM keeping the solute fixed with a positional restraint of 500 kcal mol^{-1} Å^{-2} followed by the relaxing of the entire system after the removal of restraints. In the last stage, a maximum of 1500 steps of restrained energy minimization and a combination of the steepest descent and conjugate gradient algorithms were applied by using a parabolic or linear penalty function for the NOE upper distance bonds and torsion angle restraints. The final **ZNF1**, 6-mer/**ZNF**, and **II**/**ZNF** structures were deposited in the Biological Magnetic Resonance Data Bank (BMRB) as entries 17228, 17229, and 17230, respectively, and in the Protein Data Bank (PDB) as entries 2l44, 2l45, and 2l46, respectively.

Quantum Mechanics/Molecular Mechanics (QM/MM). The starting structure of the protein and DNA was taken from

the first NMR structure. PROPKA was used to determine the protonation states of the titratable residues.[32] The binding site of platinum on the guanine was confirmed to be N7.[15] Therefore, after preoptimization of the {Pt(dien)} fragment with a model {Pt(dien)NH_3}, the inorganic complex was placed close to the N7 atom within the available space close to it. Then the system was solvated with a 30 Å water droplet that was relaxed to soak (200 ns MD) the **II** complex, which was repeated once to achieve a sufficient solvation. In total, 3494 TIP3P waters were added and only 88 in the second solvation that were all on the droplet surface. The complete system consists of 10990 atoms.

The QM/MM methodology used here has been successfully applied in many enzymatic studies with transition metals and is described in more detail in several reviews.[33−38] Briefly, the B3LYP functional was chosen for the QM part, and these calculations were performed with TURBOMOLE.[39−45] The CHARMM 35.1b force field was employed for the MM part, and these calculations were performed with DL_POLY.[46,47] The dien topology and parameters were obtained from the Swissparam website (http://swissparam.ch/). The hydrogen link atom approach with charge shift was used for the QM/MM boundary region, and the electrostatic embedding scheme also was used.[48,49] The QM/MM calculations were performed using ChemShell that links input/output from DL_POLY and also runs the HDLC optimizer.[50,51]

The QM region consists of the Pt, dien, and Gua4 moieties and therefore a total of 37 atoms. All atoms with 15 Å of the Pt ion were identified as active MM atoms, which was a total of 1705 atoms. The QM/MM structure was obtained by using the def2-TZVP basis set as implemented in TURBOMOLE.[52] The described model and basis set result in a total of 706 basis functions. For Pt, a 60-electron relativistic effective core potential was used.[53]

Molecular Dynamics. The molecular dynamics (MD) calculations were performed with CHARMM version 35b3 and the CHARMM27 force field.[46,54−57] The three different systems (free **ZF1** and 6-mer/**ZF1** and **II**/**ZF1** mixtures) were set up separately from their first NMR structures. The structures were solvated within a cubic box of TIP3P waters (3591, 3693, and 4505 waters, respectively), and the system was then neutralized with chloride and potassium ions.[58] After energy minimization, the system was heated and equilibrated for 200 ps at 300 K. The production step was run for 1 ns with the leapfrog integrator at a time step of 1 fs and under constant pressure and temperature conditions at 300 K. The SHAKE algorithm was used to constrain all hydrogen bonds.[59]

The zinc ion was placed within the tetrahedral coordination sphere formed by the three sulfur atoms from cysteines 36, 39, and 49 and the $N_{\varepsilon 2}$ atom of histidine 44. The four first-sphere ligand atoms of the zinc ion were fixed. The charge and force field parameters for the thiolate residues were used as previously published.[60]

RESULTS AND DISCUSSION

Characterization of Platinated Oligonucleotide {[Pt(dien)d(5′-TACGCC-3′)]}. The adduct ({Pt(dien)(6-mer)}) was isolated and purified by FPLC (see Experimental Procedures). ESIMS-TOF in negative mode confirmed the 1:1 adduct with two major peaks at m/z 1023 and 2049 assigned to $\{Pt(dien)(6\text{-mer})\}^{2-}$ and $\{Pt(dien)(6\text{-mer})\}^{-}$, respectively (Figure S1 of the Supporting Information).

Table 2. Selected Peptide ^{1}H NMR Chemical Shifts, at 298 K, in the 6-mer/ZF1 Mixture (I), in the II/ZF1 Mixture (II), and for free ZF1 (III)

		H	Hα	Hβ2	Hβ3	Hδ1	Hδ2	Hδ3	Hε1	Hε3	Hγ2	Hγ3	Hη2	Hζ2	Hζ3	Qβ	Qδ	Qε	Qγ
Trp37	I	8.980	4.531	3.148	3.061	6.976	–	–	9.716	7.022	–	–	6.709	6.687	6.589	–	–	–	–
	II	8.575	4.426	3.360	3.268	7.219	–	–	9.973	7.429	–	–	7.073	7.338	6.966	–	–	–	–
	III	8.469	4.394	3.342	3.438	7.315	–	–	10.07	7.577	–	–	7.203	7.466	7.108	–	–	–	–
Lys38	I	9.704	4.369	–	–	–	–	–	–	–	–	–	–	–	–	2.274	1.700	2.928	1.333
	II	9.353	4.189	–	–	–	–	–	–	–	–	–	–	–	–	2.156	1.672	2.891	1.254
	III	9.252	4.143	2.135	2.080	–	1.660	1.687	–	–	1.226	1.256	–	–	–	–	–	2.883	–
Met46	I	9.198	4.673	1.939	1.628	–	–	–	–	–	2.305	2.215	–	–	–	–	–	–	–
	II	8.919	4.732	–	–	–	–	–	–	–	2.842	2.510	–	–	–	2.178	–	–	–
	III	8.832	4.763	2.143	1.904	–	–	–	–	–	2.216	2.507	–	–	–	–	–	–	–
Lys47	I	8.887	4.148	1.849	1.730	–	–	–	–	–	1.281	1.212	–	–	–	–	1.632	–	–
	II	8.597	4.108	1.839	1.713	–	–	–	–	–	–	–	–	–	–	–	1.294	3.253	1.214
	III	8.509	4.104	–	–	–	1.590	1.706	–	–	1.217	1.304	–	–	–	1.841	–	–	–

dx.doi.org/10.1021/bi201834g | *Biochemistry* 2012, 51, 1752−1761

Figure 2. Superposition of the best 20 structures of the **ZF1** (blue), 6-mer/**ZF1** (green), and **II**/**ZF1** (orange) adducts. The 6-mer/**ZF1** structure was calculated using a total of 394 distance constraints, of which 30 were intermolecular, with an average rmsd of 0.24 Å for the backbone. When the 6-mer/**ZF1** structure was superimposed with free **ZF1**, the backbone rmsd was 0.90 Å. When the **II**/**ZF1** structure was superimposed with the other two structures, the backbone rmsd was 0.91 Å. See Table 1.

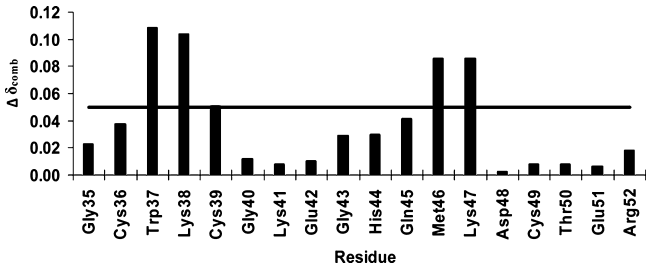

Figure 3. $\Delta\delta_{comb}$ for the **II**/**ZF1** adduct vs **ZF1**. The combined chemical shift changes were determined on the basis of directly observed ^{15}N and ^{1}H chemical shifts according to Schumann.[24] The cutoff value was calculated with the corrected standard deviation to zero σ_0^{corr}. The disposition of the tryptophan residues is summarized in Table S3 of the Supporting Information, with a summary of major deviations of the other peptide residues.

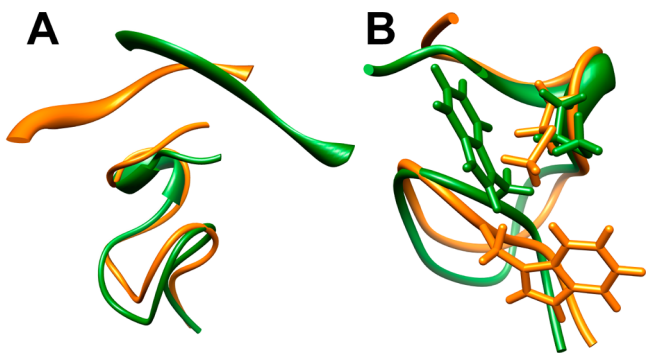

Figure 4. (A) Superposition of the minimized structures of the 6-mer/**ZF1** adduct (green) and the **II**/**ZF1** adduct (orange) showing the change in peptide conformation upon oligonucleotide platination. (B) Detail of **ZF1** denoting the change in conformation of Trp37 in the two environments.

Circular Dichroism Spectroscopy. Conformational changes from the interactions of the 6-mer and its Pt(dien) adduct, **II**, with **ZF1** were monitored by circular dichroism (CD). The CD spectra of the oligonucleotides are characterized by the presence of two positive bands at 275 and 212 nm and one slightly negative band at 242 nm. The spectrum of the free zinc finger shows two positive bands centered around 212 and 220 nm and a negative band at 200 nm, which report on peptide secondary structure and are characteristic of a *β*-sheet.[8,10] Upon incubation of **ZF1** and 6-mer, the 190−250 nm region shows a deviation from the arithmetic sum of the components, and in the presence of **II**, smaller deviations were observed. Because the spectra contain contributions from both the peptide and the oligonucleotide in this region, analysis is correspondingly more complex (Figure S3 of the Supporting Information).

NMR Spectroscopy. The 1D ^{1}H NMR spectrum of adduct **II** shows a downfield shift of the guanine H8 of approximately 0.4 ppm (8.312 ppm vs 7.891 ppm), indicating N7-guanine platination (Table S1 and Figure S2 of the Supporting Information), confirmed by the QM/MM calculations (see below). The slight downfield shifts observed for Cyt3 and Cyt5 H5/H6 also reflect their proximity to the platination site (Table S1 of the Supporting Information). Total assignments of the nonexchangeable protons were performed using NOESY data following standard procedures.[16] Some of the base protons were not assigned because of the proximity of the water signal. The sequential connectivity pattern formed by intra- and internucleotide NOEs involving the H6/H8 base and the H1′ and H2′/H2″ sugar protons in the platinated oligonucleotide is shown in Figures S4 and S5 of the Supporting Information, respectively. Some cross-peaks, such as the internucleotide Ade2 H1′−Cyt3 H6 and Cyt5 H1′−Cyt6 H6 NOEs, are missing or are very weak because of the absence of a double strand. A very strong intranucleotide H8−H1′ NOE of Gua4 confirms the *syn* nucleoside conformation, common upon platination. Interestingly, the strong intranucleotide H6−H1′ cross-peaks of Cyt3 and Cyt5 also indicate a *syn* conformation for these nucleotides. The results may be compared with those of the Pt(dien) adducts of trinucleotides d(5′-AGA) and d(5′-CGT).[61,62] In these cases, the conformational changes are sequence-dependent, with platination resulting in a G *syn* conformation for the latter but more indicative of high *anti* in the former.[61,62] Conformational changes of binding of Pt(dien) to duplex DNA have been reported,[63] but to the best of our knowledge, no extended single-stranded DNAs have been studied. The "delocalization" of conformational changes beyond the platinum binding site is reminiscent of the situation in which monofunctional platinum binding of the phase II clinical drug BBR3464 $[\{trans\text{-}PtCl(NH_3)_2\}_2\text{-}\mu\text{-}\{trans\text{-}Pt(NH_3)_2(H_2N(CH_2)_6NH_2)_2\}]^{4+}$ in formation of a 1,4-interstrand cross-link in the 8-mer d(ATG*TAC*AT}$_2$ also results in "cooperative" *anti* → *syn* conformational changes of the intervening adenine bases.[64]

The complete specific assignment of all protons corresponding to the C-terminal (34−52) finger of HIVNCp7, **ZF1**, and in presence of the free and platinated 6-mer **II** was also obtained following general procedures (Tables S2 and S3 of the Supporting Information).[16] Addition of **ZF1** induces few significant changes in the spectrum of **II**; Gua4 H8 remains downfield, confirming platination, and the cytosines remain in the same environment (Table S1 of the Supporting Information). For Gua4, the main changes are for H4′ (4.304−4.156 ppm) and H5′ and H5″ (4.040−4.200 ppm) (Table S1 of the Supporting Information). In the presence of **II**, the tryptophan resonances (except for H*β*2) are shifted

dx.doi.org/10.1021/bi201834g | *Biochemistry* 2012, 51, 1752−1761

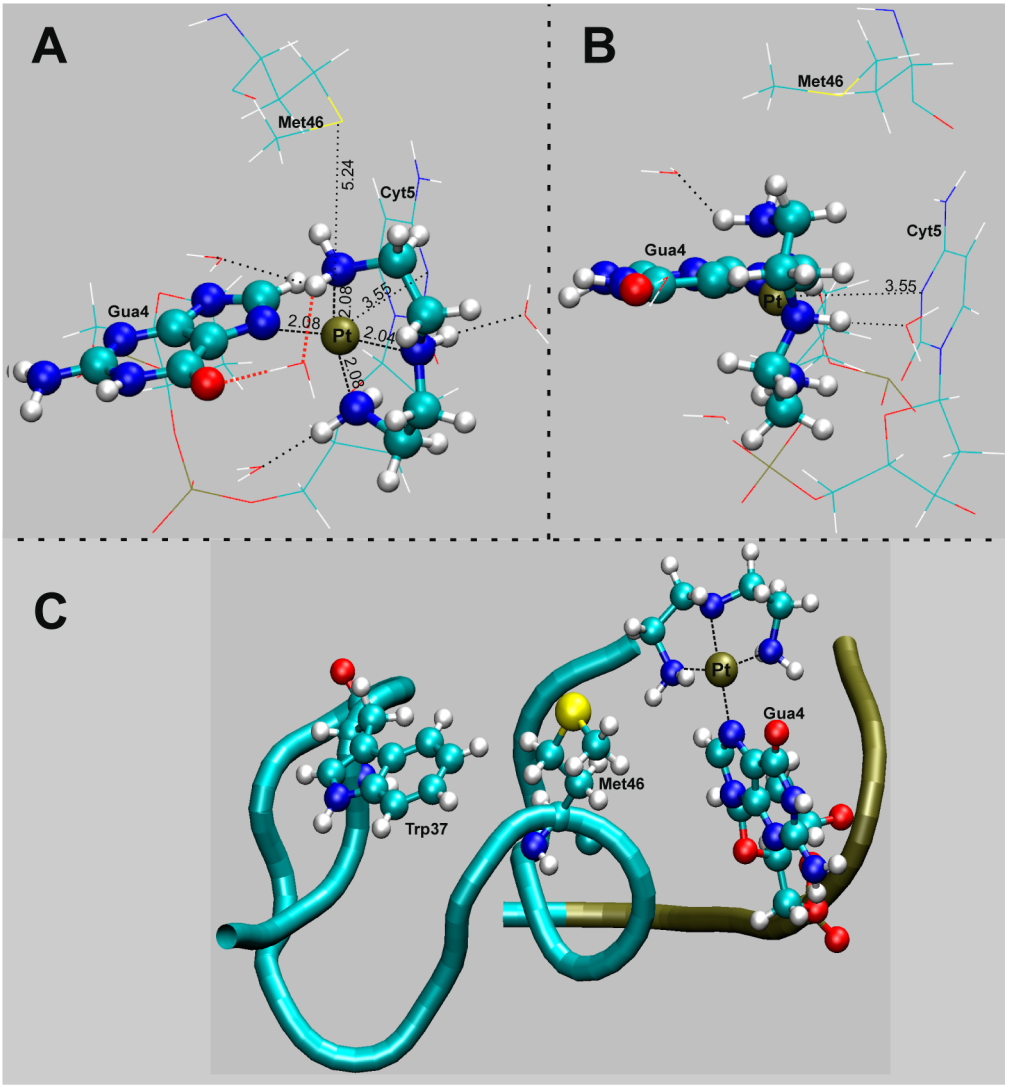

Figure 5. Optimized QM/MM structure at the B3LYP/def2-TZVP level of theory of the **II**/**ZF1** HIVNCp7 adduct. QM atoms are shown in CPK and nearby MM atoms as lines: (A) front view, (B) side view, and (C) overall view showing the most important residues. The Pt coordination sphere is square planar with three of the first-ligand sphere nitrogens being equally distant from the Pt, with the central Pt−N(dien) bond length (2.04 Å) slightly shorter than the others (2.08 Å). These results are consistent with reported Pt−nucleobase structures.[15,16]

upfield and broadened. Other major shifts are for Gln45 (Hε21, Hγ3, Qβ), Met46 (NH, Hγ2), Lys47 (NH, Qγ), and Glu50 (Hγ2, Hγ3). The Zn−Cys/His chemical shifts show only marginal deviations. The major peptide deviations are listed in Table 2.

Determination of Solution Structures. The solution structures of **ZF1** and the 6-mer/**ZF1** and **II**/**ZF1** adducts were calculated from the NOESY-derived distance constraints (Table 1 and Figure 2).[16] For the peptide in the absence of any DNA, the NMR-derived solution structures of HIV-1 nucleocapsid proteins (13−51)HIVNCp7 and (1−55)HIVNCp7 (MN strain) may be used for comparison.[26,65] **ZF1** is 100% homologous to both strains, and no appreciable differences between free **ZF1** and these structures (PDB entry 1ESK) are found (rmsd of 0.64 Å). The 6-mer/**ZF1** structure is, however, very different from that of the adduct between full HIVNCp7 and d(5′-ACGCC), where there are stabilizing interactions with the N-terminal and C-terminal fingers, and the oligonucleotide adopts an almost perpendicular orientation relative to the critical linker region between the two ZFs.[13] In the absence of the N-terminal ZF and the linker, the hexanucleotide adopts a completely different orientation (Figure S6 of the Supporting Information), although several amino acids implicated in the interaction with the nucleic acids and responsible for the stability of the complex are the same (Trp37, Gln45, and Met46). The hydrophobic interaction between Trp37 and guanine bases in interactions of NCp7 with d(5′-ACGCC-3′) and stem−loop SL3 ψ-RNA/NCp7 is a principal feature of NCp7−oligonucleotide recognition.[12−14] Here there is also an interaction between Trp37 and the ribose protons of Gua4, exemplifying the carbohydrate−aromatic ring interaction as a further important molecular recognition motif.[66] Interestingly, investigation of cTAR DNA-NC(11−55) protein contacts indicates a significant role for hydrophobic interactions involving nucleobases and deoxyribose sugars with C1′ and C2′ of the sugar moieties in contact with the aromatic side chains of Phe16 and Trp37.[67]

The chemical shift changes of **ZF1** in the presence of **II** may predict the interaction interface, with Trp37, Lys38, Met46, and Lys47 being the most affected (Table 2 and Figure 3). These

dx.doi.org/10.1021/bi201834g | *Biochemistry* 2012, 51, 1752−1761

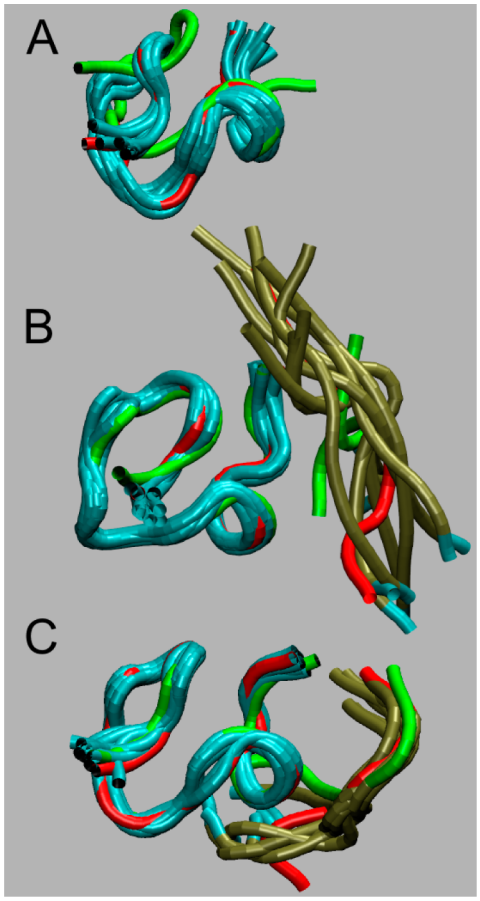

Figure 6. Overlay of 10 frames taken every 200 ps of the 2 ns MDs for (A) free **ZF1**, (B) the 6-mer/**ZF1** adduct, and (C) the **II**/**ZF1** adduct. Green denotes the starting structure from the NMR data and red the last structure at 2 ns. For each simulation, the first NMR structure was used as a starting structure. The zinc ion and Zn-coordinating atoms were kept fixed. When the Zn and the ligand atoms were free to move, the **ZF1** structure remained stable, even when an additional water molecule was included in the Zn coordination sphere. After the equilibration period, the starting structure (panel A, green) undergoes a transition into a stable conformation and does not change very much over the 2 ns of the MD. The rmsd plots are provided in the Figure S11 of the Supporting Information. Two H-bonds are present: one between the amino group of Cyt6 and the backbone ketone oxygen of the Cys49−Thr50 peptide bond and the other between the hydroxyl group of Thr50 and the ketone oxygen of Cyt6 (see also Figure 7).

shifts are accompanied by the appearance of new Met46−Cyt6 H5 and Trp37−Cyt5 H5 NOEs but severe weakening of the Trp37−Gua4 contact (Figure S7 of the Supporting Information). This loss of contact with Trp37 is attributed to the steric effects caused by Gua4 platination and is accompanied by a change in the position of the aromatic ring (Figure 4B). The position of the DNA in the **II**/**ZF1** structure is completely different than in the absence of platinum (Figure 4A).

Theoretical QM/MM calculations on the **II**/**ZF1** adduct supplemented the NMR structure description (Figures S8 and S9 of the Supporting Information). The dien ligand is rotated 90° with respect to the Gua4 residue, possibly because of (i) Cyt5 hindrance of dien rotation and (ii) H-bonds from a H_2O molecule to the Gua4 oxygen and a dien amino group (Figure 5). The Cyt5 N3 atom is in an axial position, 3.55 Å from the Pt center, closer than the Met46 sulfur (5.24 Å). This latter approximation is supported by the observed Met46−Cyt6 NOE in the **II**/**ZF1** adduct. The bulkiness of the platinated DNA adduct should be partly responsible for the change in the relative position of the free 6-mer and also for some of the conformational changes in the peptide backbone.

Finally, the protein−DNA interactions were simulated by MD (Figure 6). The atomistic level confirms the 6-mer−**ZF1** stabilizing interactions to be (i) Trp37 π-stacking with Gua4 and (ii) H-bonds between the pentose oxygens and phosphate oxygen of Cyt5 and Gua4 (Figure S10 of the Supporting Information). Upon platination, the 6-mer is less flexible and stays in one stable conformation on the **ZF1** surface (Figure 6C). The Gua4−Trp37 interaction is disrupted as expected, and instead, there are H-bonding interactions between Cyt6 and Cys49 and Thr50 (Figure 7). Additionally, the backbone CH group is close to N3 of Cyt6. Although the N···HC interaction is weak, the interatomic distance fluctuates around 2.5 Å during almost the entire 2 ns of the simulation. Via inclusion of this third H-bond, the bonding modes mimic the three intermolecular Cyt−Gua base pair H-bonds (Figure 7).

Conclusions. In conclusion, this is to the best of our knowledge the first structural characterization of platinated single-stranded DNA showing delocalized nucleoside (*anti* → *syn*) conformational changes over three bases, either side of the platination site. The results further show for the first time that platinated oligonucleotides may interact intimately with ZFs with the peptide undergoing a conformational change. In this case, strong H-bonding interactions contribute to the overall stability of the **II**/**ZF1** adduct even when the Trp−Gua π-stacking in the 6-mer/**ZF1** adduct is disrupted by the steric and conformational effects of nucleobase platination. The results further demonstrate the feasibility of targeting specific ZF motifs with DNA-tethered coordination compounds, such as Pt compounds and Co macrocycles.[8,18,19] The wide variety of nucleotide binding sites identified for NCp7[68] thus allows for suitable modulation of the platinated guanine site. The conformational changes of the single-stranded DNA could be sequence-dependent, as seen in early work with trinucleotides. DNA targeting is especially attractive for HIVNCp7, given its multiple roles in nucleic acid recognition.[3]

Protein recognition and repair of damaged DNA from intrinsic and extrinsic perturbations are critical cellular functions.[69,70] Many proteins containing the zinc finger binding motif process platinum-bound DNA.[71,72] Zinc finger proteins such as the Sp1 transcription factor and the XPA (mammalian) and UvrABC (bacterial) nucleotide excision repair complexes recognize and bind to cisplatin-damaged DNA.[73−75] In the structure described here, the distortion of the methionine suggests that, besides the Zn-bound cysteinates, suitable backbone residues may be positioned to enhance nucleophilic attack on a "saturated" or substitution-inert PtN_4 center, a novel possibility for chemical repair of platinated duplex DNA by zinc fingers. This possible chemistry would be highly dependent on both the nature of the DNA adduct (1,2/1,3-intrastrand; 1,2-interstrand) and the reactivity of the Zn coordination sphere (Cys_2His_2, Cys_3His, or Cys_4).[2,76] These considerations suggest that the study of platinated duplex DNA and zinc finger motifs is a rich area of chemistry worthy of further study.

■ ASSOCIATED CONTENT

Supporting Information

Complementary figures and tables. This material is available free of charge via the Internet at http://pubs.acs.org.

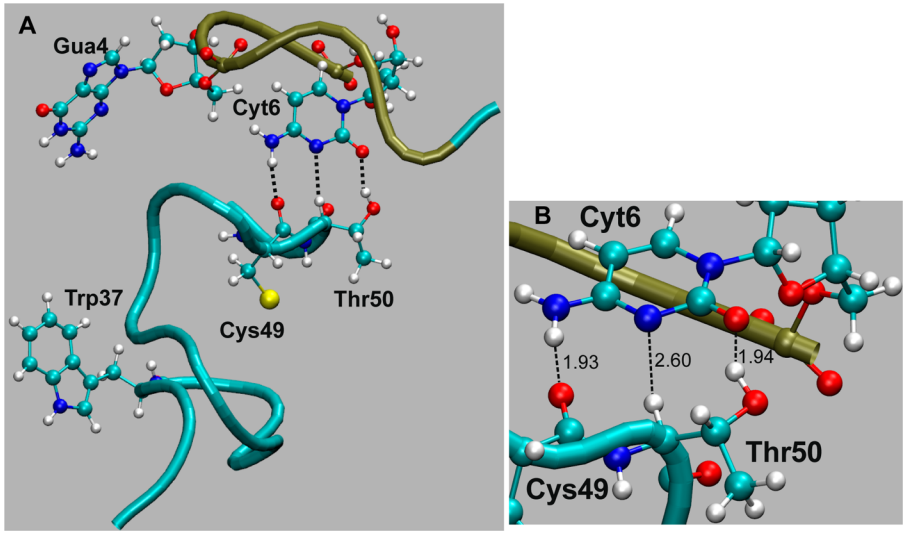

Figure 7. (A) Stabilizing interactions of Cyt6 with the protein residues, Cys49 and Thr50, in the **II**/ZF1 adduct (frame 844 ns). (B) Detail showing the H-bonds.

AUTHOR INFORMATION

Corresponding Author

*E-mail: npfarrell@vcu.edu. Phone: (804) 828-6320. Fax: (804) 828-8599.

Funding

S.Q. and A.V. thank Fundação para a Ciência e a Tecnologia-FCT (Portugal) for postdoctoral (SFRH/BPD/27454/2006) and doctoral (SFRH/BD/35992/2007) fellowships, respectively. We acknowledge the Portuguese National NMR Network (RNRMN) supported by funds from FCT. N.P.F. is thankful for National Science Foundation Grants 0616768 and CHE-1012269.

Notes

The authors declare no competing financial interest.

ACKNOWLEDGMENTS

We thank John B. Mangrum for the acquisition of mass spectra.

ABBREVIATIONS

pyr, pyridine; quin, quinoline; dien, diethylenetriamine; 9-EtGua, 9-ethylguanine; GMP, 5′-guanosine monophosphate; NOE, nuclear Overhauser effect; rmsd, root-mean-square deviation.

REFERENCES

(1) Maret, W., and Li, Y. (2009) Coordination dynamics of zinc in proteins. *Chem. Rev. 109*, 4682−4707.

(2) Quintal, S. M., dePaula, Q. A., and Farrell, N. P. (2011) Zinc finger proteins as templates for metal ion exchange and ligand reactivity. Chemical and biological consequences. *Metallomics 3*, 121−139.

(3) Levin, J. G., Guo, J., Rouzina, I., and Musier-Forsyth, K. (2005) Nucleic acid chaperone activity of HIV-1 nucleocapsid protein: Critical role in reverse transcription and molecular mechanism. *Prog. Nucleic Acid Res. Mol. Biol. 80*, 217−286.

(4) deClercq, E. (2010) Antiretroviral drugs. *Curr. Opin. Pharmacol. 10*, 507−510.

(5) Mehellou, Y., and deClercq, E. (2010) Twenty-Six Years of Anti-HIV Drug Discovery: Where Do We Stand and Where Do We Go? *J. Med. Chem. 53*, 521−538.

(6) Musah, R. A. (2004) The HIV-1 Nucleocapsid Zinc Finger Protein as a Target of Antiretroviral Therapy. *Curr. Top. Med. Chem. 4*, 1605−1622.

(7) de Rocquigny, H., Shvadchak, V., Avilov, S., Dong, C. Z., Dietrich, U., Darlix, J.-L., and Mély, Y. (2008) Targeting the viral nucleocapsid protein in anti-HIV-1 therapy. *Mini Rev. Med. Chem. 8*, 24−35.

(8) Anzellotti, A. I., Liu, Q., Bloemink, M. J., Scarsdale, J. N., and Farrell, N. (2006) Targeting retroviral Zn finger-DNA interactions: A small-molecule approach using the electrophilic nature of trans-platinum-nucleobase compounds. *Chem. Biol. 13*, 539−548.

(9) Sartori, D. A., Miller, B., Bierbach, U., and Farrell, N. (2000) Modulation of the chemical and biological properties of trans platinum complexes: Monofunctional platinum complexes containing one nucleobase as potential antiviral chemotypes. *J. Biol. Inorg. Chem. 5*, 575−583.

(10) de Paula, Q. A., Mangrum, J. B., and Farrell, N. P. (2009) Zinc finger proteins as templates for metal ion exchange: Substitution effects on the C-finger of HIV nucleocapsid NCp7 using M(chelate) species (M = Pt, Pd, Au). *J. Inorg. Biochem. 103*, 1347−1354.

(11) Bose, R. N., Wei, W., Yang, W., and Evanics, F. (2005) Structural perturbation of a C4 zinc-finger module by *cis*-diamminedichloroplatinum(II): Insights into the inhibition of transcription processes by the antitumor drug. *Inorg. Chim. Acta 358*, 2844−2854.

(12) Bourbigot, S., Ramalanjaona, N., Boudier, C., Salgado, G. F., Roques, B. P., Mély, Y., Bouaziz, S., and Morellet, N. (2008) How the HIV-1 nucleocapsid protein binds and destabilises the (−)primer binding site during reverse transcription. *J. Mol. Biol. 383*, 1112−1128.

(13) Morellet, N., Demene, H., Teilleux, V., Huynh-Dinh, T., de Rocquigny, H., Fournie-Zalusli, M. C., and Roques, B. P. (1998) Structure of the complex between the HIV-1 nucleocapsid protein NCp7 and the single-stranded pentanucleotide d(ACGCC). *J. Mol. Biol. 283* (2), 419−434.

(14) De Guzman, R. N., Wu, Z. R., Stalling, C. C., Pappalardo, L., Borer, P. N., and Summers, M. F. (1998) Structure of the HIV-1 nucleocapsid protein bound to the SL3 Psi-RNA recognition element. *Science 279*, 384−388.

(15) Anzellotti, A. I., Bayse, C. A., and Farrell, N. P. (2008) Effects of Nucleobase Metalation on Frontier Molecular Orbitals: Potential Implications for π-Stacking Interactions with Tryptophan. *Inorg. Chem. 47*, 10425−10431.

(16) Anzellotti, A. I., Sabat, M., and Farrell, N. (2006) Covalent and Noncovalent Interactions for [Metal(dien)nucleobase]$^{2+}$ Complexes with L-Tryptophan Derivatives: Formation of Palladium-Tryptophan

Species by Nucleobase Substitution under Biologically Relevant Conditions. *Inorg. Chem. 45*, 1638−1645.
(17) Schuler, W., Dong, C.-Z., Wecker, K., and Roques, B. P. (1999) NMR Structure of the complex between the zinc finger protein NCp10 of Moloney Leukemia Virus and the single-stranded pentanucleotide d(ACGCC): Comparison with HIV-NCp7 complexes. *Biochemistry 38*, 12984−12994.
(18) Louie, A. Y., and Meade, T. J. (1998) A cobalt complex that selectively disrupts the structure and function of zinc fingers. *Proc. Natl. Acad. Sci. U.S.A. 95*, 6663−6668.
(19) Harney, A. S., Lee, J., Manus, L. M., Wang, P., Ballweg, D. M., LlaBonne, C., and Meade, T. J. (2009) Targeted inhibition of Snail family zinc finger transcription factors by oligonucleotide-Co(III) Schiff base conjugate. *Proc. Natl. Acad. Sci. U.S.A. 106*, 13667−13672.
(20) Annibale, G., Brandolisio, M., and Pitteri, B. (1995) New routes for the synthesis of chloro(diethylenetriamine)platinum(II)chloride and chloro(2,2′/6′,2″-terpyridine)platinum(II) chloride dihydrate. *Polyhedron 14*, 451−453.
(21) Hwang, T. L., and Shaka, A. J. (1995) Water suppression that works. Excitation sculpting using arbitrary wave-forms and pulsed-field gradients. *J. Magn. Reson., Ser. A 112*, 275−279.
(22) Goddard, T. D., and Kneller, D. G. (2007) *SPARKY 3*, University of California, San Francisco.
(23) Wüthrich, K. (1986) *NMR of Proteins and Nucleic Acids*, John Wiley & Sons Inc., New York.
(24) Schumann, F. H., Riepl, H., Maurer, T., Gronwald, W., Neidig, K. P., and Kalbitzer, H. R. (2007) Combined chemical shift changes and amino acid specific chemical shift mapping of protein-protein interactions. *J. Biomol. NMR 39*, 275−289.
(25) Guntert, P. (2004) Automated NMR protein structure calculation with CYANA. *Methods Mol. Biol. 278*, 353−378.
(26) Summers, M. F., Henderson, L. E., Chance, M. R., Bess, J. W., South, T. L., Blake, P. R., Sagi, I., Perez-Alvarado, G., Sowder, R. C., Hare, D. R., and Arthur, L. O. (1992) Nucleocapsid zinc fingers detected in retroviruses: EXAFS studies of intact viruses and the solution-state structure of the nucleocapsid protein from HIV-1. *Protein Sci. 1* (5), 563−574.
(27) Pelton, J. G., Torchia, D. A., Meadow, N. D., and Roseman, S. (1993) Tautomeric states of the active-site histidines of phosphorylated and unphosphorylated IIIGlc, a signal-transducing protein from *Escherichia coli*, using two-dimensional heteronuclear NMR techniques. *Protein Sci. 2*, 543−558.
(28) Case, D. A., Darden, T. A., Cheatham, T. E., III, Simmerling, C. L., Wang, J., Duke, R. E., Luo, R., Merz, K. M., Pearlman, D. A., Crowley, M., Walker, R. C., Zhang, W., Wang, B., Hayik, S., Roitberg, A., Seabra, G., Wong, K. F., Paesani, F., Wu, X., Brozell, S., Tsui, V., Gohlke, H., Yang, L., Tan, C., Mongan, J., Hornak, V., Cui, G., Beroza, P., Mathews, D. H., Schafmeister, C., Ross, W. S., and Kollman, P. A. (2006) *AMBER 9*, University of California, San Francisco.
(29) Hornak, V., Abel, R., Okur, A., Strockbine, B., Roitberg, A., and Simmerling, C. (2006) Comparison of multiple Amber force fields and development of improved protein backbone parameters. *Proteins 65*, 712−725.
(30) Jorgensen, W. L., Chandrasekhar, J., Madura, J. D., Impey, R. W., and Klein, M. L. (1983) Comparison of Simple Potential Functions for Simulating Liquid Water. *J. Chem. Phys. 79*, 926−935.
(31) Darden, T., York, D., and Pedersen, L. (1993) Particle mesh Ewald: An N.Log(N) Method for Ewald sums in large systems. *J. Chem. Phys. 98*, 10089−10092.
(32) Li, H., Robertson, A. D., and Jensen, J. H. (2005) Very fast empirical prediction and rationalization of protein pK_a values. *Proteins: Struct., Funct., Bioinf. 61*, 704−721.
(33) Zheng, J., Wang, D., Thiel, W., and Shaik, S. (2006) QM/MM study of mechanisms for compound I formation in the catalytic cycle of cytochrome P450cam. *J. Am. Chem. Soc. 128*, 13204−13215.
(34) Waller, M. P., Bühl, M., Geethalakshmi, K. R., Wang, D., and Thiel, W. (2007) V-51 NMR chemical shifts calculated from QM/MM models of vanadium chloroperoxidase. *Chem.—Eur. J. 13*, 4723−4732.
(35) Metz, S., and Thiel, W. (2009) A combined QM/MM study on the reductive half-reaction of xanthine oxidase: Substrate orientation and mechanism. *J. Am. Chem. Soc. 131*, 14885−14902.
(36) Senn, H. M., and Thiel, W. (2007) QM/MM methods for biological systems. *Top. Curr. Chem. 268*, 173−290.
(37) Senn, H. M., and Thiel, W. (2009) QM/MM Methods for Biomolecular Systems. *Angew. Chem., Int. Ed. 48*, 1198−1229.
(38) Kästner, J., Thiel, S., Senn, H. M., Sherwood, P., and Thiel, W. (2007) Exploiting QM/MM capabilities in geometry optimization: A microiterative approach using electrostatic embedding. *J. Chem. Theory Comput. 3*, 1064−1072.
(39) Slater, J. C. (1951) A simplification of the Hartree-Fock method. *Phys. Rev. 81*, 385−390.
(40) Vosko, S. H., Wilk, L., and Nusair, M. (1980) Accurate spin-dependent electron liquid correlation energies for local spin-density calculations: A critical analysis. *Can. J. Phys. 58*, 1200−1211.
(41) Becke, A. D. (1988) Density-functional exchange-energy approximation with correct asymptotic-behavior. *Phys. Rev. A 38*, 3098−3100.
(42) Becke, A. D. (1993) Density-functional thermochemistry. 3. The role of exact exchange. *J. Chem. Phys. 98*, 5648−5652.
(43) Stephens, P. J., Devlin, F. J., Chabalowski, C. F., and Frisch, M. J. (1994) *Ab-initio* calculation of vibrational absorption and circular-dichroism spectra using density-functional force-fields. *J. Phys. Chem. 98*, 11623−11627.
(44) Lee, C. T., Yang, W. T., and Parr, R. G. (1988) Development of the Colle-Salvetti correlation-energy formula into a functional of the electron density. *Phys. Rev. B 37*, 785−789.
(45) Ahlrichs, R., Bär, M., Häser, M., Horn, H., and Kölmel, C. (1989) Electronic-structure calculations on workstation computers: The program system turbomole. *Chem. Phys. Lett. 162*, 165−169.
(46) Brooks, B. R., Brooks, C. L. III, Mackerell, A. D., Nilsson, L., Petrella, R. J., Roux, B., Won, Y., Archontis, G., Bartels, C., Boresch, S., Caflisch, A., Caves, L., Cui, Q., Dinner, A. R., Feig, M., Fischer, S., Gao, J., Hodoscek, M., Im, W., Kuczera, K., Lazaridis, T., Ma, J., Ovchinnikov, V., Paci, E., Pastor, R. W., Post, C. B., Pu, J. Z., Schaefer, M., Tidor, B., Venable, R. M., Woodcock, H. L., Wu, X., Yang, W., York, D. M., and Karplus, M. (2009) CHARMM: The Biomolecular Simulation Program. *J. Comput. Chem. 30*, 1545−1615.
(47) Smith, W., and Forester, T. R. (1996) DL_POLY_2.0: A general-purpose parallel molecular dynamics simulation package. *J. Mol. Graphics 14*, 136−141.
(48) Sherwood, P., de Vries, A. H., Collins, S. J., Greatbanks, S. P., Burton, N. A., Vincent, M. A., and Hillier, I. H. (1997) Computer simulation of zeolite structure and reactivity using embedded cluster methods. *Faraday Discuss. 106*, 79−92.
(49) Bakowies, D., and Thiel, W. (1996) Hybrid models for combined quantum mechanical and molecular mechanical approaches. *J. Phys. Chem. 100*, 10580−10594.
(50) Sherwood, P., de Vries, A. H., Guest, M. F., Schreckenbach, G., Catlow, C. R. A., French, S. A., Sokol, A. A., Bromley, S. T., Thiel, W., Turner, A. J., Billeter, S., Terstegen, F., Thiel, S., Kendrick, J., Rogers, S. C., Casci, J., Watson, M., King, F., Karlsen, E., Sjovoll, M., Fahmi, A., Schafer, A., and Lennartz, C. (2003) QUASI: A general purpose implementation of the QM/MM approach and its application to problems in catalysis. *THEOCHEM 632*, 1−28.
(51) Billeter, S. R., Turner, A. J., and Thiel, W. (2000) Linear scaling geometry optimization and transition state search in hybrid delocalised internal coordinates. *Phys. Chem. Chem. Phys. 2*, 2177−2186.
(52) Weigend, F., and Ahlrichs, R. (2005) Balanced basis sets of split valence, triple ζ valence and quadruple ζ valence quality for H to Rn: Design and assessment of accuracy. *Phys. Chem. Chem. Phys. 7*, 3297−3305.
(53) Andrae, D., Haeussermann, U., Dolg, M., Stoll, H., and Preuss, H. (1990) Energy-adjusted *ab-initio* pseudopotentials for the 2nd and 3rd row transition-elements. *Theor. Chim. Acta 77*, 123−141.
(54) MacKerell, A. D. Jr., Feig, M., and Brooks, C. L. III (2004) Extending the treatment of backbone energetics in protein force fields: Limitations of gas-phase quantum mechanics in reproducing protein

conformational distributions in molecular dynamics simulations. *J. Comput. Chem. 25*, 1400−1415.
(55) MacKerell, A. D. Jr., Bashford, D., Bellott, M., Dunbrack, R. L. Jr., Evanseck, J. D., Field, M. J., Fischer, S., Gao, J., Guo, H., Ha, S., Joseph-McCarthy, D., Kuchnir, L., Kuczera, K., Lau, F. T. K., Mattos, C., Michnick, S., Ngo, T., Nguyen, D. T., Prodhom, B., Reiher, W. E. III, Roux, B., Schlenkrich, M., Smith, J. C., Stote, R., Straub, J., Watanabe, M., Wiórkiewicz-Kuczera, J., Yin, D., and Karplus, M. (1998) All-atom empirical potential for molecular modeling and dynamics studies of proteins. *J. Phys. Chem. B 102*, 3586−3616.
(56) Foloppe, N., and MacKerell, A. D. Jr. (2000) All-atom empirical force field for nucleic acids: I. Parameter optimization based on small molecule and condensed phase macromolecular target data. *J. Comput. Chem. 21*, 86−104.
(57) MacKerell, A. D. Jr., and Banavali, N. (2000) All-atom empirical force field for nucleic acids: II. Application to molecular dynamics simulations of DNA and RNA in solution. *J. Comput. Chem. 21*, 105−120.
(58) Jorgensen, W. L., Chandrasekhar, J., Madura, J. D., Impey, R. W., and Klein, M. L. (1983) Comparison of simple potential functions for simulating liquid water. *J. Chem. Phys. 79*, 926−935.
(59) Ryckaert, J. P., Ciccotti, G., and Berendsen, H. J. C. (1977) Numerical-integration of cartesian equations of motion of a system with constraints: Molecular dynamics of n-alkanes. *J. Comput. Phys. 23*, 327−341.
(60) Foloppe, N., Sagemark, J., Nordstrand, K., Berndt, K. D., and Nilsson, L. (2001) Structure, dynamics and electrostatics of the active site of glutaredoxin 3 from *Escherichia coli*: Comparison with functionally related proteins. *J. Mol. Biol. 310*, 449−470.
(61) Admiraal, G., Alink, M., Altona, C., Dijt, F. J., van Garderen, C. J., de Graaf, R. A. G., and Reedijk, J. (1992) Conformation of Pt(dien)[d(ApGpA)-N7(2)] in the solid state and aquesous solution, as determined with single-crystal X-ray diffraction and high-resolution NMR spectroscopy in solution. *J. Am. Chem. Soc. 114*, 930−938.
(62) van Garderen, C. J., Altona, C., and Reedijk, J. (1988) Alterations in the d(CpGpT) structure in solution as a result of $[PtCl(diethylenetriamine)]^+$ binding. *Eur. J. Biochem. 178*, 115−121.
(63) Brabec, V., Reedijk, J., and Leng, M. (1992) Sequence-dependent distortions induced in DNA by monofunctional platinum-(II) binding. *Biochemistry 31*, 12397−12402.
(64) Qu, Y., Scarsdale, N. J., Tran, M.-C., and Farrell, N. (2003) Cooperative effects in long-range 1,4 DNA-DNA interstrand cross-links formed by polynuclear platinum complexes. An unexpected *syn*-orientation of adenine bases outside the binding sites. *J. Biol. Inorg. Chem. 8*, 19−28.
(65) Morellet, N., Jullian, N., de Rocquigny, H., Maigret, B., Maigret, J. L., and Roques, B. P. (1992) Determination of the structure of the nucleocapsid protein NCP7 from the human-immunodeficiency-virus type-1 by H-1-NMR. *EMBO J. 11* (8), 3059−3065.
(66) Fernandez-Alonso, M. C., Cañada, F. J., Jiménez-Barbero, J., and Cuevas, G. (2005) Molecular recognition of saccharides by proteins. Insights on the origin of the carbohydrate-aromatic interactions. *J. Am. Chem. Soc. 127*, 7379−7386.
(67) Bazzi, A., Zargarian, L., Chaminade, F., Boudier, C., De Rocquigny, H., René, B., Mély, Y., Fossé, P., and Mauffret, O. (2011) Structural insights into the cTAR DNA recognition by the HIV-1 nucleocapsid protein: Role of sugar deoxyribose in the binding polarity of NC. *Nucleic Acids Res. 39*, 3903−3916.
(68) Darlix, J.-L., Godet, J., Ivany-Nagy, R., Fossé, P., Mauffret, O., and Mély, Y. (2011) Flexible nature and specific functions of the HIV-1 nucleocapsid protein. *J. Mol. Biol. 410*, 565−581.
(69) Sancar, A. (1996) DNA excision repair. *Annu. Rev. Biochem. 65*, 43−81.
(70) Croteau, D. L., Peng, Y., and Van Houten, B. (2008) DNA repair gets physical: Mapping an XPA-binding site on ERCC1. *DNA Repair 7*, 819−826.
(71) Kartalou, M., and Essigmann, J. M. (2001) Recognition of cisplatin adducts by cellular proteins. *Mutat. Res. 478*, 1−21.
(72) Wang, D., and Lippard, S. J. (2005) Cellular processing of platinum anticancer drugs. *Nat. Rev. Drug Discovery 4*, 307−320.
(73) Buchanan, R. L., and Gralla, J. D. (1990) Cisplatin resistance and mechanism in a viral test system: SV40 isolates that resist inhibition by the antitumor drug have lost regulatory DNA. *Biochemistry 29*, 3436−3442.
(74) Truglio, J. J., Croteau, D. L., and Van Houten, B. (2006) Prokaryotic nucleotide excision repair: The UvrABC system. *Chem. Rev. 106*, 233−252.
(75) Jones, C. J., and Wood, R. D. (1993) Preferential binding of the Xeroderma Pigmentosum group A complementing protein to damaged DNA. *Biochemistry 32*, 12096−12104.
(76) Maynard, A. T., Huang, M., Rice, W. G., and Covell, D. G. (1998) Reactivity of the HIV-1 nucleocapsid protein p7 zinc finger domains from the perspective of density-functional theory. *Proc. Natl. Acad. Sci. U.S.A. 95*, 11578−11583.